Int J Mech Mater Des (2016) 12:463–476
DOI 10.1007/s10999-015-9327-9

Dual reciprocity boundary element method using compactly supported radial basis functions for 3D linear elasticity with body forces

Cheuk-Yu Lee · Hui Wang · Qing-Hua Qin

Received: 29 June 2015 / Accepted: 13 October 2015 / Published online: 28 October 2015

Abstract A new computational model by integrating the boundary element method and the compactly supported radial basis functions (CSRBF) is developed for three-dimensional (3D) linear elasticity with the presence of body forces. The corresponding displacement and stress particular solution kernels across the supported radius in the CSRBF are obtained for inhomogeneous term interpolation. Subsequently, the classical dual reciprocity boundary element method, in which the domain integrals due to the presence of body forces are transferred into equivalent boundary integrals, is formulated by introducing locally supported displacement and stress particular solution kernels for solving the inhomogeneous 3D linear elastic system. Finally, several examples are presented to demonstrate the accuracy and efficiency of the present method.

Dr. Wang is currently visiting at ANU.

C.-Y. Lee · H. Wang · Q.-H. Qin (✉)
Research School of Engineering, Australian National University, Acton, ACT 2601, Australia
e-mail: Qinghua.qin@anu.edu.au

C.-Y. Lee
e-mail: cheuk.lee@anu.edu.au

H. Wang
e-mail: huiwang_china@163.com

H. Wang
Department of Engineering Mechanics, Henan University of Technology, Zhengzhou 450001, China

Keywords Three-dimensional linear elasticity · Dual reciprocity method · Boundary element method · Compactly supported radial basis functions

1 Introduction

It is noted that for 3D linear elasticity with the presence of arbitrary body forces, analytical solutions are available only for a few problems with very simple geometries, boundary conditions and body force terms such as gravitational forces (Piltner 1987; Wang and Zheng 1995; Qin and Mai 1997; Qin 2000; Qin and Ye 2004; Barber 2006; Lee et al. 2008). In most cases, as irregular geometries or boundaries are involved, numerical solutions are usually sought. Numerical methods such as the finite element method (FEM), the finite difference method (FDM) and the boundary element/integral method (BEM/BIM) provide alternative approaches to approximate the 3D elasticity solutions in the past decades (Jirousek et al. 1995; Qin and Mai 2002; Qin 2003, 2005; Bathe 2006). Among them, the FEM and the FDM require domain discretization while the BEM/BIM requires only boundary discretisation for the homogeneous partial differential equations (PDE) and thus has advantage of dimension reduction over the FEM/FDM. However, domain discretisation is generally unavoidable in the BEM/BIE for the inhomogeneous PDE problems like the 3D linear elasticity problems with arbitrary body forces under consideration. To make the BEM a truly

boundary discretisation method for the inhomogeneous cases, a variety of domain transformation methods such as the radial integration method (RIM; Gao 2002) and the dual reciprocity boundary element method (DRBEM; Nardini and Brebbia 1983) have been proposed to obtain equivalent boundary terms and bypass the need of domain integration caused by the inhomogeneous terms. The essence of the former method is to transform the domain integral into surface integral consisting of radial integral function while the latter method aims to directly interpolate the inhomogeneous terms by a series of linearly independent basis functions and then analytically determines the respected particular solution kernels. In both methods, the choice of the basis functions is critical to provide accurate numerical solutions (Golberg et al. 1998; Wang and Qin 2007). In most of the literatures, the usual choices are the globally supported radial basis function (RBF). For example, the DRBEM traditionally uses the linear radial basis functions $1 + r$ for inhomogeneous term interpolation (Wang and Qin 2006). More recently, successful RBF applications to 3D linear elasticity problems include the globally supported Gaussian (Coleman et al. 1991) and the thin plate spline $r^2 \log(r)$, augmented with the additional terms of a Pascal triangle expansion (Bridges and Wrobel 1996; Partridge and Sensale 1997; Partridge 2000; Qin and Wang 2008).

However, the choice of globally supported RBF has been questioned in relation to the accuracy and the number and position of internal nodes required to obtain satisfactory results, especially for irregular domains. The severe drawback of using the above globally supported RBFs is their dense interpolation matrices, which often become highly ill-conditioned as the number of interpolation points or the order of basis functions increases. Conversely, RBFs with locally supported feature such as the Wendland's CSRBF are capable of producing sparse interpolation matrices and improving matrix conditioning while maintaining competitive accuracy (Wendland 1995, 1998; Natalini and Popov 2006). As the result, CSRBF has become a natural choice for solving higher dimensional problems (Golberg et al. 2000; Tsai 2001; Chen et al. 2003). To our best knowledge, the application of the CSRBF has only been applied to two-dimensional elasticity problems by Rashed (2002a, b).

In this paper, the dual reciprocity boundary element formulation with CSRBF approximation is developed for 3D linear elasticity with arbitrary body forces. In our approach, we consider using the dual reciprocity technique to convert the domain integrals due to the presence of body forces in the boundary element formulation into equivalent boundary integrals and the CSRBF instead of the conventional globally supported basis functions for the dual reciprocity approximation. During the computation, we can freely control the sparseness of the interpolation matrix by varying the support radius without trading off too much of the accuracy. Using Galerkin vectors in the linear elastic theory, the important particular solution kernels with respect to the CSRBF approximation (Lee et al. 2015) are firstly reviewed for completeness. Subsequently, the coefficients associated with the particular solution kernels are determined by the addition of internal nodes and the full solutions are evaluated by the DRBEM formulation. Finally, several examples are presented to demonstrate the accuracy and efficiency of the present method.

The remainder of this paper is organized as follows. Section 2 describes the basics of three-dimensional elasticity. Section 3 presents the concept of the particular solution kernels associated with the Wendland's CSRBF, and in Sect. 4, the formulation of dual reciprocity boundary element method with CSRBF is presented. Several examples are considered in Sect. 5. Finally, some concluding remarks on the present method are presented in Sect. 6.

2 Problem description

Consider a 3D isotropic linear elastic body with inhomogeneous body force terms in the domain Ω. The governing equations are

$$\sigma_{ij,j}(\boldsymbol{x}) + b_i(\boldsymbol{x}) = 0 \quad \boldsymbol{x} \in \Omega \tag{1}$$

$$\sigma_{ij}(\boldsymbol{x}) = \lambda\varepsilon_{kk}(\boldsymbol{x})\delta_{ij} + 2G\varepsilon_{ij}(\boldsymbol{x}) \quad \boldsymbol{x} \in \Omega \tag{2}$$

$$\varepsilon_{ij}(\boldsymbol{x}) = \frac{1}{2}\left(u_{i,j}(\boldsymbol{x}) + u_{j,i}(\boldsymbol{x})\right) \quad \boldsymbol{x} \in \Omega \tag{3}$$

where $\boldsymbol{x}$ is a point in the domain Ω, σ_{ij} the stress tensor, ε_{ij} the strain tensor, u_i the displacement vector, b_i the known body force vector, λ and G the Lame constants and δ the Kronecker delta. Herein and after, an index after a comma denotes a differentiation with respect to the coordinate component corresponding to the index.

Combining the above equations yields the following Navier's equations in terms of displacement components

$$\mathcal{L}(u_i) + b_i(\boldsymbol{x}) = 0 \quad \boldsymbol{x} \in \Omega \tag{4a}$$

with the differential operator $\mathcal{L}$

$$\mathcal{L}(u_i) = Gu_{i,jj}(\boldsymbol{x}) + \frac{G}{1-2v}u_{j,ij}(\boldsymbol{x}) \tag{4b}$$

where v is the Poisson's ratio which can be expressed as $v = \frac{\lambda}{2(\lambda+G)}$. Later in the numerical examples, Young modulus E and Poisson's ratio v will be employed, in which G can be computed using the conversion formula $G = \frac{E}{2(1+v)}$.

Besides, for a direct problem with the linear elastic governing equations, the corresponding boundary conditions should be supplemented for the determination of the unknown displacement and stress fields. The boundary conditions considered in this work include:

- Displacement boundary condition

$$u_i(\boldsymbol{x}) = \bar{u}_i(\boldsymbol{x}) \quad \boldsymbol{x} \in \Gamma_u \tag{5a}$$

- Traction boundary condition

$$t_i(\boldsymbol{x}) = \sigma_{ij}(\boldsymbol{x})n_j(\boldsymbol{x}) = \bar{t}_i(\boldsymbol{x}) \quad \boldsymbol{x} \in \Gamma_t \tag{5b}$$

where t_i is the traction field, $\bar{u}_i$ and $\bar{t}_i$ the prescribed displacement and traction, n_i the unit vector outward normal to the boundary Γ_t. It is assumed as usual that the boundaries Γ_u and Γ_t are not overlapped so that $\Gamma = \Gamma_u \cup \Gamma_t$ and $\emptyset = \Gamma_u \cap \Gamma_t$.

3 Dual reciprocity method

In order to determine the particular solution, it is convenient to express the particular solutions of displacement u_i^p in terms of Galerkin vector g_i as (Fung 1965).

$$u_i^p(\boldsymbol{x}) = g_{i,kk}(\boldsymbol{x}) - \frac{1}{2(1-v)}g_{k,ik}(\boldsymbol{x}) \quad \boldsymbol{x} \in \Omega \tag{6}$$

Upon substituting Eq. (6) into Eq. (4) yields the following bi-harmonic equation

$$g_{i,jjkk}(\boldsymbol{x}) = -\frac{b_i(\boldsymbol{x})}{G} \quad \boldsymbol{x} \in \Omega \tag{7}$$

By means of derivation of displacement variables, the corresponding stress particular solutions in terms of Galerkin vector is

$$\sigma_{ij}(\boldsymbol{x}) = \frac{G}{1-v}\left[vg_{k,mmk}(\boldsymbol{x})\delta_{ij} - g_{k,ijk}(\boldsymbol{x}) + (1-v)\left(g_{i,jkk}(\boldsymbol{x}) + g_{j,ikk}(\boldsymbol{x})\right)\right] \quad \boldsymbol{x} \in \Omega \tag{8}$$

Sometimes, inhomogeneous terms of Eq. (7) could be a well described function such as gravitational load, for which special particular solution can be found analytically (Fam and Rashed 2005). In many other cases, finding such analytical solution is not a trivial task. The dual reciprocity method (DRM) aims to efficiently approximate the particular solution by finding its solution kernels while prescribing the inhomogeneous terms such as body forces with a series of linearly independent basis functions so that any known or unknown body forces terms can be reconstructed using finite set of discrete data

$$b_i(\boldsymbol{x}) \approx \sum_{n=1}^{N} \alpha_l^n \delta_{li}\varphi_n(\boldsymbol{x}) \quad \boldsymbol{x} \in \Omega \tag{9a}$$

where φ_n is the chosen series of basis functions to approximate body forces from the inhomogeneity terms of Eq. (7), N the number of interpolation points including the boundary points and interior points, α_l^n the interpolation coefficients to be determined. The use of the Kronecker delta δ is to separate the basis functions for approximating the body forces in each direction independently, i.e.

Similarly, the Galerkin vector g_i and the particular solution u_i^p, σ_{ij}^p and t_i^p can be expressed as

$$\begin{bmatrix} \varphi_1(\boldsymbol{x}) & 0 & 0 & \varphi_2(\boldsymbol{x}) & 0 & 0 & \cdots & \varphi_N(\boldsymbol{x}) & 0 & 0 \\ 0 & \varphi_1(\boldsymbol{x}) & 0 & 0 & \varphi_2(\boldsymbol{x}) & 0 & \cdots & 0 & \varphi_N(\boldsymbol{x}) & 0 \\ 0 & 0 & \varphi_1(\boldsymbol{x}) & 0 & 0 & \varphi_2(\boldsymbol{x}) & \cdots & 0 & 0 & \varphi_N(\boldsymbol{x}) \end{bmatrix} \begin{Bmatrix} \alpha_1^1 \\ \alpha_2^1 \\ \alpha_3^1 \\ \alpha_1^2 \\ \alpha_2^2 \\ \alpha_3^2 \\ \vdots \\ \alpha_1^N \\ \alpha_2^N \\ \alpha_3^N \end{Bmatrix} = \begin{Bmatrix} b_1(\boldsymbol{x}) \\ b_2(\boldsymbol{x}) \\ b_3(\boldsymbol{x}) \end{Bmatrix} \tag{9b}$$

$$g_i(\boldsymbol{x}) = \sum_{n=1}^{N} \alpha_l^n \delta_{li} \phi_n(\boldsymbol{x}) \quad \boldsymbol{x} \in \Omega \tag{10a}$$

$$u_i^p(\boldsymbol{x}) = \sum_{n=1}^{N} \alpha_l^n \psi_{li}^n(\boldsymbol{x}) \quad \boldsymbol{x} \in \Omega \tag{10b}$$

$$\sigma_{ij}^p(\boldsymbol{x}) = \sum_{n=1}^{N} \alpha_l^n S_{lij}^n(\boldsymbol{x}) \quad \boldsymbol{x} \in \Omega \tag{10c}$$

$$t_i^p(\boldsymbol{x}) = \sum_{n=1}^{N} \alpha_l^n n_j(\boldsymbol{x}) S_{lij}^n(\boldsymbol{x}) \quad \boldsymbol{x} \in \Omega \tag{10d}$$

where ϕ_n is the respected Galerkin vector solution kernels, ψ_{li}^n the displacement particular solution kernels, S_{lij}^n the stress particular solution kernels.

By linearity, it suffices to analytically determine ϕ_n by substituting Eqs. (9) and (10a) into Eq. (7)

$$\phi_{n,jjkk}(\boldsymbol{x}) = -\frac{\varphi_n(\boldsymbol{x})}{G} \quad \boldsymbol{x} \in \Omega \tag{11}$$

It's clear that by enforcing Eq. (7) to satisfy the known inhomogeneity terms in the domain Ω, we can obtain N linear equations to uniquely solve for the interpolation coefficients α_l^n.

Generally, the function φ in Eq. (11) can be chosen as radial basis function such that

$$\varphi_j(\boldsymbol{x}_i) = \varphi(\boldsymbol{x}_i - \boldsymbol{x}_j) = \varphi(r_{ij}) \tag{12}$$

where $\boldsymbol{x}_i$ represents the collocation points and $\boldsymbol{x}_j$ represents the reference points.

Herein, RBF is employed to approximate the inhomogeneous terms of Eq. (7), as done in some literatures (Golberg and Chen 1998; Golberg et al. 2000; Rashed 2002a; Wang and Qin 2008). Since RBF is expressed in terms of Euclidian distance r, it usually works well in arbitrary dimensional space and doesn't increase computational cost. Furthermore, many attractive properties of RBF such as good convergence power, positive definiteness and ease of smoothness control are widely reported (Buhmann 2003; Wendland 2005).

To analytically determine ϕ, ψ_{li} and S_{lij}, an explicit function needs to be chosen first for φ. For Wendland's CSRBF in 3D (Wendland 1995, 1998), φ is defined as

$$\varphi(r) = \left(1 - \frac{r}{\alpha}\right)_+^2 = \begin{cases} \left(1 - \frac{r}{\alpha}\right)^2 & 0 \le r \le \alpha \\ 0 & r > \alpha \end{cases} \quad \text{for } C^0 \text{ smoothness} \tag{13a}$$

$$\varphi(r) = \left(1 - \frac{r}{\alpha}\right)_+^4 \left(4\frac{r}{\alpha} + 1\right) \quad \text{for} \quad C^2 \text{ smoothness} \tag{13b}$$

$$\varphi(r) = \left(1 - \frac{r}{\alpha}\right)_+^6 \left(35\left(\frac{r}{\alpha}\right)^2 + 18\frac{r}{\alpha} + 3\right) \quad \text{for } C^4 \text{ smoothness} \tag{13c}$$

$$\varphi(r) = \left(1 - \frac{r}{\alpha}\right)_+^8 \left(35\left(\frac{r}{\alpha}\right)^3 + 25\left(\frac{r}{\alpha}\right)^2 + 8\frac{r}{\alpha} + 1\right) \quad \text{for} \quad C^6 \text{ smoothness} \tag{13d}$$

where the subscript + denotes that the bracket function will be forced to be zero when the bracketed value is less than zero. α is a cut off parameter for varying the support radius of interpolation matrix $\varphi(r)$ as illustrated in Fig. 1.

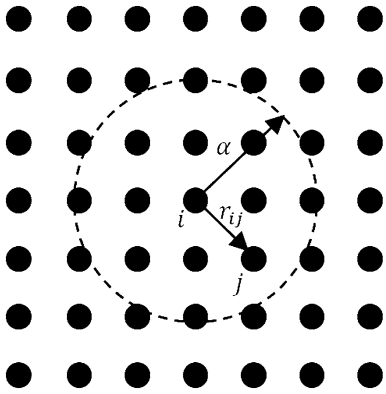

Fig. 1 Cut off parameter α for various support radii

The sparseness of the CSRBF interpolation matrix can be interpreted as the cumulative frequency of r, which is defined as

$$sparseness = \sum_{i}^{N}\sum_{j}^{N} f(r_{ij})\left[r_{ij} \le \alpha\right] \tag{14a}$$

with

$$f(r) = \sum_{i}^{N}\sum_{j}^{N} \frac{\left[r = r_{ij}\right]}{N^2} \tag{14b}$$

where f is the frequency function of r_{ij} and [] denotes the use of Iverson Bracket. For case $\alpha = \max(r)$, sparseness of the interpolation matrix is equal to 100 %. For case $\alpha = 0$, the sparseness is equal to 0 %. In practice α can be chosen according to the sparseness requirement.

Meanwhile, the related particular solution using compactly supported functions can be derived (Lee et al. 2015). Here, their formulations are provided in "Appendix".

4 Formulation of dual reciprocity boundary element method

In the classical BEM, the domain integral arises due to the presence of body forces is illustrated in Eq. (15)

$$\begin{aligned} &c_{ij}u_j(\boldsymbol{x_P}) + \oint_S T_{ij}(\boldsymbol{x_P},\boldsymbol{x_Q})u_j(\boldsymbol{x_Q})dS(\boldsymbol{x_Q}) \\ &\quad - \int_S U_{ij}(\boldsymbol{x_P},\boldsymbol{x_Q})t_j(\boldsymbol{x_Q})dS(\boldsymbol{x_Q}) \\ &\quad = \int_V U_{ij}(\boldsymbol{x_P},\boldsymbol{x_Q})b_j(\boldsymbol{x_Q})dV(\boldsymbol{x_Q}) \end{aligned} \tag{15}$$

where U_{ij} and T_{ij} are the fundamental solutions for displacements and surface tractions, respectively, $\boldsymbol{x_P}$ is a source point which can be any point within the domain or on the boundary, $\boldsymbol{x_Q}$ is an arbitrary integration point and c_{ij} are the boundary geometry coefficient (Qin and Huang 1990; Gao and Davies 2002).

$$c_{ij} = \delta_{ij} + \lim_{\boldsymbol{x_Q}\to\boldsymbol{x_P}} \int_S T_{ij}(\boldsymbol{x_P},\boldsymbol{x_Q})dS(\boldsymbol{x_Q}) \tag{16}$$

The dual reciprocity method makes use of the particular solution kernels from Eq. (10b), in which the domain integral containing the body forces term becomes

$$\begin{aligned} &\int_V U_{ij}(\boldsymbol{x_P},\boldsymbol{x_Q})b_j(\boldsymbol{x_Q})dV(\boldsymbol{x_Q}) \\ &\quad = -\int_V \mathcal{L}\left(u_j^p(\boldsymbol{x_Q})\right)U_{ij}(\boldsymbol{x_P},\boldsymbol{x_Q})dV(\boldsymbol{x_Q}) \\ &\quad = -\sum_{n=1}^{N}\alpha_l^n \int_V \mathcal{L}(\psi_{li}^n(\boldsymbol{x_Q}))U_{ij}(\boldsymbol{x_P},\boldsymbol{x_Q})dV(\boldsymbol{x_Q}) \end{aligned} \tag{17}$$

Integrating by parts the differential operator term yields

$$\begin{aligned} &\int_V U_{ij}(\boldsymbol{x_P},\boldsymbol{x_Q})b_j(\boldsymbol{x_Q})dV(\boldsymbol{x_Q}) \\ &\quad = \sum_{n=1}^{N}\alpha_l^n\left(c_{ij}\psi_{lj}^n(\boldsymbol{x_P}) + \oint_S T_{ij}(\boldsymbol{x_P},\boldsymbol{x_Q})\psi_{lj}^n(\boldsymbol{x_Q})dS(\boldsymbol{x_Q})\right. \\ &\quad \left. - \int_S U_{ij}(\boldsymbol{x_P},\boldsymbol{x_Q})n_j(\boldsymbol{x_Q})S_{lij}^n(\boldsymbol{x_Q})dS(\boldsymbol{x_Q})\right) \end{aligned} \tag{18}$$

Substituting Eq. (18) in Eq. (15), we have

$$\begin{aligned} &c_{ij}u_j(\boldsymbol{x_P}) + \oint_S T_{ij}(\boldsymbol{x_P},\boldsymbol{x_Q})u_j(\boldsymbol{x_Q})dS(\boldsymbol{x_Q}) \\ &\quad - \int_S U_{ij}(\boldsymbol{x_P},\boldsymbol{x_Q})t_j(\boldsymbol{x_Q})dS(\boldsymbol{x_Q}) \\ &\quad = \sum_{n=1}^{N}\alpha_l^n\left(\begin{array}{l} c_{ij}\psi_{lj}^n(\boldsymbol{x_P}) + \oint_S T_{ij}(\boldsymbol{x_P},\boldsymbol{x_Q})\psi_{lj}^n(\boldsymbol{x_Q})dS(\boldsymbol{x_Q}) \\ \quad - \int_S U_{ij}(\boldsymbol{x_P},\boldsymbol{x_Q})n_j(\boldsymbol{x_Q})S_{lij}^n dS(\boldsymbol{x_Q}) \end{array}\right) \end{aligned} \tag{19}$$

Next, to write Eq. (19) in discretised form, the whole boundary is modelled with E surface elements so that we can use summations over the boundary

elements to replace the integrals in Eq. (19). For example, the first two terms in Eq. (19) can be written in discretised form as

$$c_{ij}u_j(\boldsymbol{x_P}) + \oint_S T_{ij}(\boldsymbol{x_P},\boldsymbol{x_Q})u_j(\boldsymbol{x_Q})dS = c_{ij}u_j(\boldsymbol{x_P}) + \sum_{e=1}^{E}\oint_{S_e} T_{ij}(\boldsymbol{x_P},\boldsymbol{x_Q})u_j(\boldsymbol{x_Q})dS(\boldsymbol{x_Q}) \tag{20}$$

where S_e is the surface of eth boundary element.

Further, introducing the interpolation functions and numerically integrating over each boundary surface element, one gets for the surface integral in Eq. (20)

$$\sum_{e=1}^{E}\sum_{g_1=1}^{G}\sum_{g_2=1}^{G} T_{ij}\left(\boldsymbol{x_P},\boldsymbol{x_e}(P_{g_1},P_{g_2})\right) \left(\sum_{n=1}^{N} N^n(P_{g_1},P_{g_2})\hat{u}_j^{en}\right) J_\xi(P_{g_1},P_{g_2})W_{g_1}W_{g_2} \tag{21}$$

where $\boldsymbol{x_e}(P_{g_1},P_{g_2}) = \boldsymbol{e_m}\sum_{n=1}^{N} N^n(P_{g_1},P_{g_2})\hat{x}_m^{en}$.

The $\boldsymbol{e_m}$ denotes the standard basis for each of the directions m in the Cartesian coordinate system, N^n is the element shape functions, $\hat{x}_j^{en}$, $\hat{u}_j^{en}$ are element nodal coordinates and displacements, respectively, J_ξ is the determinant of the local Jacobian matrix related to the global coordinate to local coordinate derivatives, P_{g_1}, P_{g_2} are element natural coordinates of integration points, G is the number of integration points, and W_{g_1}, W_{g_2} are the associated weight factors.

After substituting Eq. (21) into Eq. (20) and replacing the local nodal indices $\hat{x}_j^{en}$ and $\hat{u}_j^{en}$ with global indices $\hat{x}_j^{k}$ and $\hat{u}_j^{k}$, we have, for p collocation points

$$\left[\delta_{pk}c_{ij}^{pk} + \sum_{g_1=1}^{G}\sum_{g_2=1}^{G} H_{ij}^{pk}(P_{g_1},P_{g_2})J_\xi(P_{g_1},P_{g_2})W_{g_1}W_{g_2}\right]\hat{u}_j^k \tag{22}$$

$$\text{where } H_{ij}^{pk}(P_{g_1},P_{g_2}) = H_{ij}^{en}(\boldsymbol{x_p},P_{g_1},P_{g_2}) = T_{ij}\left(\boldsymbol{x_p},\boldsymbol{x_e}(P_{g_1},P_{g_2})\right)N^n(P_{g_1},P_{g_2}). \tag{23}$$

Similar procedure can be applied for the third integral term in Eq. (19). Finally, one obtains the following expression in matrix form

$$\mathbf{H'u} - \mathbf{Gt} = \left(\mathbf{H'\hat{U}} - \mathbf{G\hat{T}}\right)\boldsymbol{\alpha} \tag{24}$$

Equation (24) is the basis for the application of the DRBEM for solving 3D linear elasticity with body forces and involves discretization of the boundary only. Moreover, the displacement and traction fundamental solutions used in the above derivation are written as (Rashed 2002a).

$$U_{li}(\boldsymbol{x_P},\boldsymbol{x_Q}) = \frac{(3-4\nu)\delta_{li} + r_{,l}r_{,i}}{16\pi G(1-\nu)r} \tag{25a}$$

$$T_{li}(\boldsymbol{x_P},\boldsymbol{x_Q}) = \frac{-1}{8\pi(1-\nu)r^2}\left[\left[(1-2\nu)\delta_{li} + 3r_{,l}r_{,i}\right]\frac{\partial r}{\partial n} - (1-2\nu)\left(r_{,l}n_{,i} - r_{,i}n_{,l}\right)\right] \tag{25b}$$

5 Numerical examples and discussions

To demonstrate the accuracy and efficiency of the derived formulation, three brenchmark examples, which are solved by the proposed method, are considered in this section. These examples include: (1) a prismatic bar subjected to gravitational load, (2) a thick cylinder under centrifugal load, and (3) axle bearing under internal pressure and gravitational load. For simplification, only Wendland's CSRBF with smoothness C^0 is considered here. Simulation results obtained from the proposed method and the conventional FEM method are compared against the analytical solutions. We also compute the mean absolute percentage error (MAPE) as an effective description for quantifying the average performance accuracy of the present method

$$MAPE = \frac{1}{n_t}\sum_{i=1}^{n_t}\left|\frac{(f_{simulation})_i}{(f_{analytical})_i} - 1\right| \times 100\,\% \tag{26}$$

where $f_{analytical}$ and $f_{simulation}$ are the analytical and simulation values evaluated at test point i. n_t is the total number of the test points.

5.1 Prismatic bar subjected to gravitational load

In the first example, we consider a straight prismatic bar subjected to gravitational load, as shown in Fig. 2. The dimensions of the bar are 1 m × 1 m × 2 m and it is fixed at the top. Assuming the bar being loaded along the z-direction by its gravitational load, the corresponding body forces can be expressed as

$$b_x = 0, \quad b_y = 0, \quad b_z = \rho g \tag{27}$$

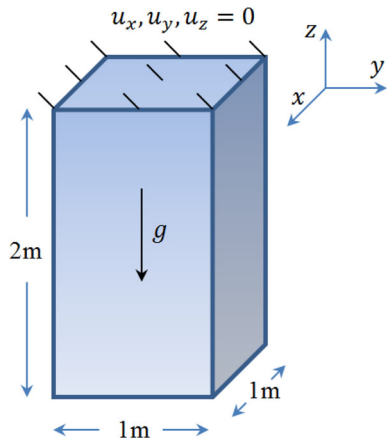

Fig. 2 Prismatic bar under gravitational load

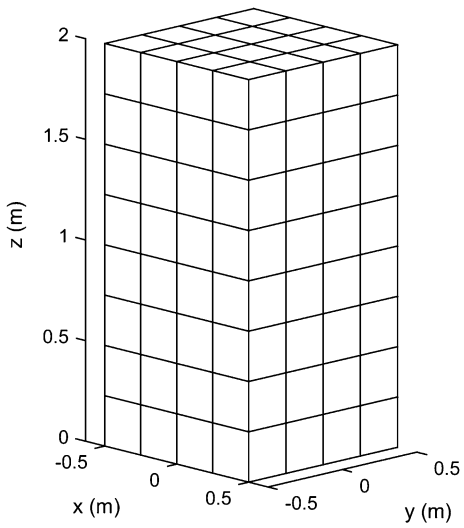

Fig. 3 Boundary element meshing of prismatic bar

where ρ is density and g is gravity. The material parameters used in the simulation are: $E = 4 \times 10^7$ Pa, $v = 0.25$, $\rho = 2000\,\mathrm{kg\,m^{-3}}$, $g = 10\,\mathrm{m\,s^{-2}}$.

The numerical model is composed of 160 boundary elements as shown in Fig. 3. Test points are chosen along the centreline of the prismatic bar. The corresponding displacement and stress results are compared to the analytical solutions (Partridge et al. 1992; Sadd 2014) and the FEM solutions, which are evaluated by the commercial software ABAQUS. Numerical results in Tables 1 and 2 show the variations of displacement and stress in terms of the sparseness of CSRBF. It is found that there is good agreement between the numerical results from the present method and the FEM results and the available analytical solutions.

5.2 Thick cylinder under centrifugal load

In the second example, a cylinder with 10 m internal radius, 10 m thickness and 20 m height is assumed to be subjected to centrifugal load. Due to the rotation, this cylinder is subjected to apparent generalized body force. If the cylinder is assumed to rotate about its z-axis as shown in Fig. 4, the generalized body forces in terms of spatial coordinates can be written as

$$b_x = \rho w^2 x, \quad b_y = \rho w^2 y, \quad b_z = 0 \tag{28}$$

where w is the angular velocity. In this example, $w = 10$ is chosen.

The problem is solved with dimensionless material parameters $E = 2.1 \times 10^5$, $v = 0.3$, $\rho = 1$. According to the symmetry of the model, only one quarter of

Table 1 Displacement results for the prismatic bar

z (m)	$-u_z(10^{-3}\,\mathrm{m})$				
	Present method			ABAQUS	Analytical solutions
	Sparseness = 20 %	Sparseness = 60 %	Sparseness = 100 %		
−0.25	0.2354	0.2314	0.2249	0.2055	0.2345
−0.50	0.4781	0.4760	0.4476	0.4141	0.4375
−0.75	0.6733	0.6422	0.6206	0.5944	0.6100
−1.00	0.8218	0.8141	0.7672	0.7392	0.7500
−1.25	0.9371	0.9238	0.8754	0.8500	0.8600
−1.50	1.0008	0.9871	0.9403	0.9285	0.9450
−1.75	1.0611	1.0431	0.9919	0.9754	0.9900
MAPE (%)	7.3808	5.5058	0.5330	3.728	

Table 2 Stress results for the prismatic bar numerical simulation

z (m)	σ_{zz} (kPa)				
	Present method			ABAQUS	Analytical solutions
	Sparseness = 20 %	Sparseness = 60 %	Sparseness = 100 %		
−0.25	39.07	36.46	35.61	36.30	35.6
−0.50	31.64	31.84	30.21	31.81	30.0
−0.75	27.51	27.07	25.05	25.91	25.0
−1.00	21.73	21.38	20.04	20.31	20.0
−1.25	15.80	15.13	15.00	15.08	15.0
−1.50	10.16	10.31	10.07	10.01	10.0
−1.75	5.66	5.61	5.42	5.00	5.0
MAPE (%)	7.72	5.70	1.46	1.975	

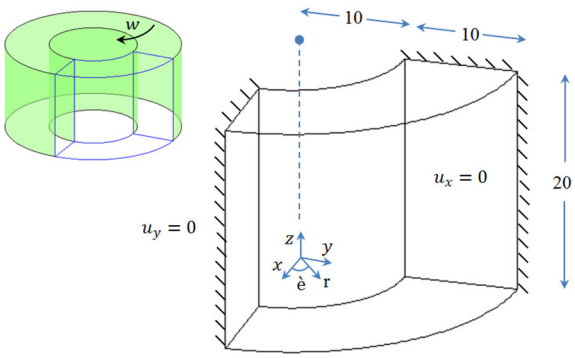

Fig. 4 Thick cylinder under centrifugal load

the cylinder domain needs to be considered for establishing the computing model. Proper symmetric displacement constraints are then applied on the symmetric planes (see Fig. 4).

The numerical model is composed of 460 boundary elements as shown in Fig. 5. For the rotating cylinder, the displacement and the stress fields are more complicated than those in the straight prismatic bar and the cantilever beam as discussed above. The results of radial and hoop stresses and radial displacement at specified locations are tabulated respectively from the present method (see Tables 3, 4, 5). These results are then compared to ABAQUS with 10,881 elements of type 20-node quadratic brick elements and the analytical solutions (Partridge et al. 1992; Sadd 2014). The result shows that the accuracy of the DRM–BEM method improves with an increase of the sparseness for the body force terms.

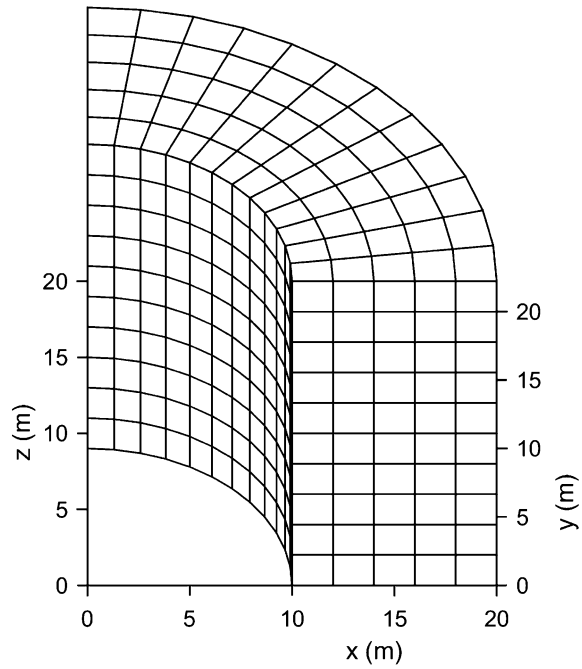

Fig. 5 Boundary element meshing of a quarter thick cylinder

5.3 Axle bearing under internal pressure and gravitational load

To show the ability of the present method for complicated geometrical domain, a numerical model of axle bearing, as taken from (Gao and Davies 2002), is used for the third example. In this model, the displacements are fixed along the boundary surface at the lower right of the bearing as shown in Fig. 6 while normal stress of 1GPa is uniformly applied to the surface of the top inner circle. Gravitational loading is

Table 3 σ_r results for the thick cylinder numerical simulation

r	σ_r (kPa)				
	Present method			ABAQUS	Analytical solutions
	Sparseness = 20 %	Sparseness = 60 %	Sparseness = 100 %		
11.25	2.57	2.52	2.40	2.434	2.367
12.50	3.93	3.87	3.68	3.740	3.620
13.75	4.47	4.37	4.17	4.233	4.099
15.00	4.33	4.25	4.04	4.108	4.010
16.25	3.77	3.71	3.52	3.568	3.484
17.50	2.87	2.83	2.69	2.647	2.604
18.75	1.54	1.51	1.44	1.442	1.430
MAPE (%)	8.6125	6.6752	1.5096	2.394	

Table 4 σ_t results for the thick cylinder numerical simulation

r	σ_t (kPa)				
	Present method			ABAQUS	Analytical solutions
	Sparseness = 20 %	Sparseness = 60 %	Sparseness = 100 %		
11.25	33.26	33.19	31.43	31.48	30.66
12.50	30.07	29.39	28.05	28.24	27.47
13.75	27.19	26.77	25.13	25.55	24.86
15.00	24.32	24.45	22.91	23.21	22.61
16.25	22.88	22.10	20.79	21.10	20.60
17.50	20.47	18.73	18.73	19.12	18.74
18.75	19.17	17.02	17.04	17.21	16.97
MAPE (%)	9.735	5.512	1.188	2.392	

Table 5 u_r results for the thick cylinder numerical simulation

r	u_r (m)				
	Present method			ABAQUS	Analytical solutions
	Sparseness = 20 %	Sparseness = 60 %	Sparseness = 100 %		
11.25	1.7382	1.7027	1.6213	1.641	1.604
12.50	1.7107	1.6837	1.5951	1.606	1.571
13.75	1.6666	1.6466	1.5656	1.582	1.547
15.00	1.6440	1.6272	1.5410	1.563	1.529
16.25	1.6410	1.6106	1.5388	1.546	1.513
17.50	1.6228	1.5927	1.5135	1.529	1.497
18.75	1.6020	1.5611	1.4908	1.510	1.477
MAPE (%)	8.2626	6.3893	1.1916	2.225	

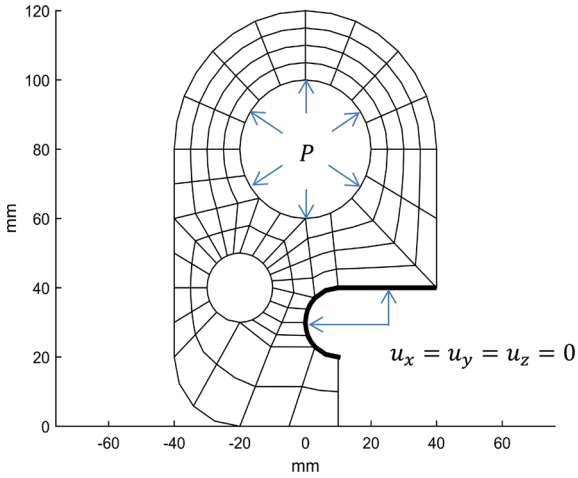

Fig. 6 Numerical model of the axle bearing

applied as similar to Eq. (27). This numerical model is meshed by 392 boundary elements as shown in Fig. 6.

The results are compared to ABAQUS and listed in Tables 6 and 7. Test points are chosen along the vertical center line from the tip of the body to the tip of the upper inner circle. Again, the result shows that the present method is as accurate as ABAQUS while requiring less computational resources.

6 Conclusion

In this study, the dual reciprocity boundary element method using compactly supported radial basis functions is developed to enrich the application of 3D isotropic linear elasticity with the presence of body forces. The particular solution kernels using the CSRBF interpolation for inhomogeneous body forces are derived using the Galerkin vectors and then coupled with equivalent boundary element integrals based on the dual reciprocity method in the solution domain. Numerical results presented in this paper demonstrate that the proposed method is capable of solving three-dimensional solid mechanics problems with inhomogeneous terms efficiently in addition to obtaining high accuracy with varied degrees of sparseness. In contrast to the globally

Table 6 Displacement results for the axle bearing numerical simulation

y (m)	u_y (10^{-3} m)			
	Present method			ABAQUS
	Sparseness = 20 %	Sparseness = 60 %	Sparseness = 100 %	
0.04	−1.7544	−1.7341	−1.6974	−1.7214
0.05	−6.4197	−6.3919	−6.3255	−6.1702
0.06	−18.1341	−17.6372	−17.4276	−17.2109
0.10	70.3576	69.1086	67.7661	67.0053
0.11	58.9133	57.7927	56.7390	56.0975
0.12	53.9164	52.9418	51.8259	51.3768

Table 7 Stress results at various test points

y (m)	σ_{xx} (MPa)			
	Present method			ABAQUS
	Sparseness = 20 %	Sparseness = 60 %	Sparseness = 100 %	
0.04	13.1720	12.7956	12.6637	12.4969
0.05	40.5788	39.8536	39.1310	38.6931
0.06	62.8807	61.7737	60.4393	59.8852
0.10	66.8648	65.5202	64.3152	63.6428
0.11	49.1604	48.1644	47.2435	46.7450
0.12	38.4089	37.5319	36.7898	36.4924

supported RBF, the CSRBF interpolation can provide stable and efficient computational treatment of various body forces and complicated geometrical domains. Moreover, the particular solution kernels derived in this paper are directly applicable to other boundary-type methods for determining particular solutions related to inhomogeneous terms in the solution domain.

Compliance with ethical standards

Conflict of interest The authors declare that they have no conflict of interest.

Appendix

The DRM particular solution using compactly supported functions are derived in our previous paper (Lee et al. 2015) and are provided here.

- For C^0 smoothness

$$\psi_{li,0\le r\le\alpha}(r) = -\frac{r^2\left(84r_{,i}r_{,l}-378\delta_{li}+420\delta_{li}v\right)}{2520G(v-1)} - \frac{r^2\left(126\delta_{li}r^2v-117\delta_{li}r^2+36r_{,i}r_{,l}r^2\right)}{2520G\alpha^2(v-1)} + \frac{\alpha r^2\left(105r_{,i}r_{,l}r-385\delta_{li}r+420\delta_{li}rv\right)}{2520G\alpha^2(v-1)}$$

$$\psi_{li,r>\alpha}(r) = \frac{\alpha^2(175\delta_{li}-210\delta_{li}v)}{2520G(v-1)} - \frac{\alpha^2\left(2\alpha^3\delta_{li}-6\alpha^3r_{,i}r_{,l}\right)}{2520Gr^3(v-1)} - \frac{\alpha^2r^2\left(63\alpha\delta_{li}+21\alpha r_{,i}r_{,l}-84\alpha\delta_{li}v\right)}{2520Gr^3(v-1)}$$

$$S_{lij,0\le r\le\alpha}(r) = -\frac{r\left(\delta_{li}r_{,j}-\delta_{ij}r_{,l}+\delta_{lj}r_{,i}\right)\left(10\alpha^2-15\alpha r+6r^2\right)}{30\alpha^2} - \frac{r\left(28\alpha^2\delta_{li}r_{,j}-112\alpha^2\delta_{ij}r_{,l}+28\alpha^2\delta_{lj}r_{,i}-72\delta_{ij}r_{,l}r^2+12\delta_{li}r_{,j}r^2+12\delta_{lj}r_{,i}r^2\right)}{420\alpha^2(v-1)} - \frac{r\left(24r_{,i}r_{,j}r_{,l}r^2+175\alpha\delta_{ij}r_{,l}r-35\alpha\delta_{li}r_{,j}r-35\alpha\delta_{lj}r_{,i}r-35\alpha r_{,i}r_{,j}r_{,l}r\right)}{420\alpha^2(v-1)}$$

$$S_{lij,r>\alpha}(r) = \frac{\alpha^3\left(\delta_{li}r_{,j}-\delta_{ij}r_{,l}+\delta_{lj}r_{,i}+3r_{,i}r_{,j}r_{,l}+2\delta_{ij}r_{,l}v-2\delta_{li}r_{,j}v-2\delta_{lj}r_{,i}v\right)}{60r^2(v-1)} + \frac{\alpha^5\left(\delta_{ij}r_{,l}+\delta_{li}r_{,j}+\delta_{lj}r_{,i}-5r_{,i}r_{,j}r_{,l}\right)}{210r^4(v-1)}$$

- For C^2 smoothness

$$\psi_{li,0\le r\le\alpha}(r) = -\frac{r^2\left(84r_{,i}r_{,l}-378\delta_{li}+420\delta_{li}v\right)}{2520G(v-1)} - \frac{r^2\left(180\delta_{li}r^5v-171\delta_{li}r^5+63r_{,i}r_{,l}r^5\right)}{2520G\alpha^5(v-1)} + \frac{\alpha r^2\left(900\delta_{li}r^4v-850\delta_{li}r^4+300r_{,i}r_{,l}r^4\right)}{2520G\alpha^5(v-1)} + \frac{\alpha^3r^2\left(1260\delta_{li}r^2v-1170\delta_{li}r^2+360r_{,i}r_{,l}r^2\right)}{2520G\alpha^5(v-1)} - \frac{\alpha r^2\left(900\delta_{li}r^4v-850\delta_{li}r^4+300r_{,i}r_{,l}r^4\right)}{2520G\alpha^5(v-1)} + \frac{\alpha^3r^2\left(1260\delta_{li}r^2v-1170\delta_{li}r^2+360r_{,i}r_{,l}r^2\right)}{2520G\alpha^5(v-1)} - \frac{\alpha^2r^2\left(1680\delta_{li}r^3v-1575\delta_{li}r^3+525r_{,i}r_{,l}r^3\right)}{2520G\alpha^5(v-1)}$$

$$\psi_{li,r>\alpha}(r) = \frac{\alpha^2(150\delta_{li}-180\delta_{li}v)}{2520G(v-1)} - \frac{\alpha^2\left(\alpha^3\delta_{li}-3\alpha^3r_{,i}r_{,l}\right)}{2520Gr^3(v-1)} - \frac{\alpha^2r^2\left(45\alpha\delta_{li}+15\alpha r_{,i}r_{,l}-60\alpha\delta_{li}v\right)}{2520Gr^3(v-1)}$$

$$
\begin{aligned}
S_{lij,0\le r\le\alpha}(r) = &-\frac{r\left(\delta_{li}r_{,j}-\delta_{ij}r_{,l}+\delta_{lj}r_{,i}\right)\left(14\alpha^5-84\alpha^3r^2+140\alpha^2r^3-90\alpha r^4+21r^5\right)}{42\alpha^5}\\
&-\frac{r\left(28\alpha^5\delta_{li}r_{,j}-112\alpha^5\delta_{ij}r_{,l}+28\alpha^5\delta_{lj}r_{,i}-189\delta_{ij}r_{,l}r^5+21\delta_{li}r_{,j}r^5+21\delta_{lj}r_{,i}r^5+800\alpha\delta_{ij}r_{,l}r^4\right)}{420\alpha^5(v-1)}\\
&-\frac{r\left(-100\alpha\delta_{li}r_{,j}r^4-100\alpha\delta_{lj}r_{,i}r^4+105r_{,i}r_{,j}r_{,l}r^5-1225\alpha^2\delta_{ij}r_{,l}r^3+175\alpha^2\delta_{li}r_{,j}r^3+175\alpha^2\delta_{lj}r_{,i}r^3\right)}{420\alpha^5(v-1)}\\
&-\frac{r\left(720\alpha^3\delta_{ij}r_{,l}r^2-120\alpha^3\delta_{li}r_{,j}r^2-120\alpha^3\delta_{lj}r_{,i}r^2+525\alpha^2r_{,i}r_{,j}r_{,l}r^3-240\alpha^3r_{,i}r_{,j}r_{,l}r^2-400\alpha r_{,i}r_{,j}r_{,l}r^4\right)}{420\alpha^5(v-1)}
\end{aligned}
$$

$$
\begin{aligned}
S_{lij,r>\alpha}(r) = &\frac{\alpha^3\left(\delta_{li}r_{,j}-\delta_{ij}r_{,l}+\delta_{lj}r_{,i}+3r_{,i}r_{,j}r_{,l}+2\delta_{ij}r_{,l}v-2\delta_{li}r_{,j}v-2\delta_{lj}r_{,i}v\right)}{84r^2(v-1)}\\
&+\frac{\alpha^5\left(\delta_{ij}r_{,l}+\delta_{li}r_{,j}+\delta_{lj}r_{,i}-5r_{,i}r_{,j}r_{,l}\right)}{420r^4(v-1)}
\end{aligned}
$$

- For C^4 smoothness

$$
\begin{aligned}
\psi_{li,0\le r\le\alpha}(r) = &-\frac{r^2}{G(v-1)}\left(\frac{r_{,i}r_{,l}}{10}-\frac{9\delta_{li}}{20}+\frac{\delta_{li}v}{2}\right)\\
&-\frac{r^2}{G\alpha^8(v-1)}\left(\frac{7\delta_{li}r^8v}{22}-\frac{175\delta_{li}r^8}{572}+\frac{35r_{,i}r_{,l}r^8}{286}\right)\\
&+\frac{\alpha r^2}{G\alpha^8(v-1)}\left(\frac{32\delta_{li}r^7v}{15}-\frac{92\delta_{li}r^7}{45}+\frac{4r_{,i}r_{,l}r^7}{5}\right)\\
&+\frac{\alpha^6r^2}{G\alpha^8(v-1)}\left(\frac{7\delta_{li}r^2v}{5}-\frac{13\delta_{li}r^2}{10}+\frac{2r_{,i}r_{,l}r^2}{5}\right)\\
&+\frac{\alpha^3r^2}{G\alpha^8(v-1)}\left(8\delta_{li}r^5v-\frac{38\delta_{li}r^5}{5}+\frac{14r_{,i}r_{,l}r^5}{5}\right)\\
&-\frac{\alpha^4r^2}{G\alpha^8(v-1)}\left(5\delta_{li}r^4v-\frac{85\delta_{li}r^4}{18}+\frac{5r_{,i}r_{,l}r^4}{3}\right)\\
&-\frac{\alpha^2r^2}{G\alpha^8(v-1)}\left(\frac{35\delta_{li}r^6v}{6}-\frac{245\delta_{li}r^6}{44}+\frac{70r_{,i}r_{,l}r^6}{33}\right)
\end{aligned}
$$

$$
\begin{aligned}
\psi_{li,r>\alpha}(r) = &\frac{\alpha^2(3575\delta_{li}-4290\delta_{li}v)}{25740G(v-1)}\\
&-\frac{\alpha^2\left(16\alpha^3\delta_{li}-48\alpha^3r_{,i}r_{,l}\right)}{25740Gr^3(v-1)}\\
&-\frac{\alpha^2r^2\left(936\alpha\delta_{li}+312\alpha r_{,i}r_{,l}-1248\alpha\delta_{li}v\right)}{25740Gr^3(v-1)}
\end{aligned}
$$

$$
\begin{aligned}
S_{lij,0\le r\le\alpha}(r) = {} & \frac{4r^3\left(\delta_{ij}r_{,l}-6\delta_{li}r_{,j}-6\delta_{lj}r_{,i}+2r_{,i}r_{,j}r_{,l}-7\delta_{ij}r_{,l}v+7\delta_{li}r_{,j}v+7\delta_{lj}r_{,i}v\right)}{5\alpha^2(v-1)} \\
& -\frac{r\left(\delta_{ij}r_{,l}-4\delta_{li}r_{,j}-4\delta_{lj}r_{,i}-5\delta_{ij}r_{,l}v+5\delta_{li}r_{,j}v+5\delta_{lj}r_{,i}v\right)}{5(v-1)} \\
& -\frac{10r^5\left(\delta_{ij}r_{,l}-8\delta_{li}r_{,j}-8\delta_{lj}r_{,i}+4r_{,i}r_{,j}r_{,l}-9\delta_{ij}r_{,l}v+9\delta_{li}r_{,j}v+9\delta_{lj}r_{,i}v\right)}{3\alpha^4(v-1)} \\
& +\frac{28r^6\left(\delta_{ij}r_{,l}-9\delta_{li}r_{,j}-9\delta_{lj}r_{,i}+5r_{,i}r_{,j}r_{,l}-10\delta_{ij}r_{,l}v+10\delta_{li}r_{,j}v+10\delta_{lj}r_{,i}v\right)}{5\alpha^5(v-1)} \\
& -\frac{140r^7\left(\delta_{ij}r_{,l}-10\delta_{li}r_{,j}-10\delta_{lj}r_{,i}+6r_{,i}r_{,j}r_{,l}-11\delta_{ij}r_{,l}v+11\delta_{li}r_{,j}v+11\delta_{lj}r_{,i}v\right)}{33\alpha^6(v-1)} \\
& +\frac{8r^8\left(\delta_{ij}r_{,l}-11\delta_{li}r_{,j}-11\delta_{lj}r_{,i}+7r_{,i}r_{,j}r_{,l}-12\delta_{ij}r_{,l}v+12\delta_{li}r_{,j}v+12\delta_{lj}r_{,i}v\right)}{5\alpha^7(v-1)} \\
& -\frac{(35r^9(\delta_{i}jr_{(,l)}-12\delta_{l}ir_{(,j)}-12\delta_{l}jr_{(,i)}+8r_{(,i)}r_{(,j)}r_{(,l)}-13\delta_{i}jr_{(,l)}v+13\delta_{l}ir_{(,j)}v+13\delta_{ljr(,i)v})}{143\alpha^8(v-1)}
\end{aligned}
$$

$$
\begin{aligned}
S_{lij,r>\alpha}(r) = {} & \frac{4\alpha^3\left(\delta_{li}r_{,j}-\delta_{ij}r_{,l}+\delta_{lj}r_{,i}+3r_{,i}r_{,j}r_{,l}+2\delta_{ij}r_{,l}v-2\delta_{li}r_{,j}v-2\delta_{lj}r_{,i}v\right)}{165r^2(v-1)} \\
& +\frac{8\alpha^5\left(\delta_{ij}r_{,l}+\delta_{li}r_{,j}+\delta_{lj}r_{,i}-5r_{,i}r_{,j}r_{,l}\right)}{2145r^4(v-1)}
\end{aligned}
$$

References

Barber, J.R.: Three-dimensional elasticity solutions for isotropic and generally anisotropic bodies. Appl. Mech. Mater. **5–6**, 541–550 (2006)

Bathe, K.J.: Finite Element Procedures. Klaus-Jurgen Bathe, United States of America (2006)

Bridges, T.R., Wrobel, L.C.: A dual reciprocity formulation for elasticity problems with body forces using augmented thin plate splines. Commun. Numer. Methods Eng. **12**, 209–220 (1996)

Buhmann, M.D.: Radial Basis Functions: Theory and Implementations. Cambridge University Press, Cambridge (2003)

Chen, C.S., Kuhn, G., Li, J., Mishuris, G.: Radial basis functions for solving near singular Poisson problems. Commun. Numer. Methods Eng. **19**, 333–347 (2003)

Coleman, C.J., Tullock, D.L., Phan-Thien, N.: An effective boundary element method for inhomogeneous partial differential equations. Z. Angew. Math. Phys. **42**, 730–745 (1991)

Fam, G.S.A., Rashed, Y.F.: The Method of Fundamental Solutions applied to 3D structures with body forces using particular solutions. Comput. Mech. **36**, 245–254 (2005)

Fung, Y.C.: Foundations of Solid Mechanics. Prentice Hall, Englewood Cliffs (1965)

Gao, X.W.: The radial integration method for evaluation of domain integrals with boundary-only discretization. Eng. Anal. Bound. Elem. **26**, 905–916 (2002)

Gao, X.W., Davies, T.G.: Boundary Element Programming in Mechanics. Cambridge University Press, Cambridge (2002)

Golberg, M.A., Chen, C.S.: The method of fundamental solutions for potential, Helmholtz and diffusion problems. In: Golberg, M.A. (ed.) Boundary Integral Methods-Numerical and Mathematical Aspects, pp. 103–176. WIT Press, Southampton (1998)

Golberg, M.A., Chen, C.S., Bowman, H., Power, H.: Some comments on the use of radial basis functions in the dual reciprocity method. Comput. Mech. **22**, 61–69 (1998)

Golberg, M.A., Chen, C.S., Ganesh, M.: Particular solutions of 3D Helmholtz-type equations using compactly supported radial basis functions. Eng. Anal. Bound. Elem. **24**, 539–547 (2000)

Jirousek, J., Wroblewski, A., Qin, Q.H., He, X.Q.: A family of quadrilateral hybrid-Trefftz p-elements for thick plate analysis. Comput. Methods Appl. Mech. Eng. **127**, 315–344 (1995)

Lee, C.Y., Qin, Q.H., Wang, H.: Trefftz functions and application to 3D elasticity. Comput. Assist. Mech. Eng. Sci. **15**, 251–263 (2008)

Lee, C.Y., Wang, H., Qin, Q.H.: Method of fundamental solutions for 3D elasticity with body forces by coupling compactly supported radial basis functions. Eng. Anal. Bound. Elem. **60**, 123–136 (2015)

Nardini, D., Brebbia, C.A.: A new approach to free vibration analysis using boundary elements. Appl. Math. Model. **7**, 157–162 (1983)

Natalini, B., Popov, V.: Tests of radial basis functions in the 3D DRM-MD. Commun. Numer. Methods Eng. **22**, 13–22 (2006)

Partridge, P.W.: Towards criteria for selecting approximation functions in the dual reciprocity method. Eng. Anal. Bound. Elem. **24**, 519–529 (2000)

Partridge, P.W., Sensale, B.: Hybrid approximation functions in the dual reciprocity boundary element method. Commun. Numer. Methods Eng. **13**, 83–94 (1997)

Partridge, P.W., Brebbia, C.A., Wrobel, L.C.: The Dual Reciprocity Boundary Element Method. Computational Mechanics Publications, Southampton (1992)

Piltner, R.: The use of complex valued functions for the solution of three-dimensional elasticity problems. J. Elast. **18**, 191–225 (1987)

Qin, Q.H.: General solutions for thermopiezoelectrics with various holes under thermal loading. Int. J. Solids Struct. **37**, 5561–5578 (2000)

Qin, Q.H.: Variational formulations for TFEM of piezoelectricity. Int. J. Solids Struct. **40**, 6335–6346 (2003)

Qin, Q.H.: Trefftz finite element method and its applications. Appl. Mech. Rev. **58**, 316–337 (2005)

Qin, Q.H., Huang, Y.Y.: BEM of postbuckling analysis of thin plates. Appl. Math. Model. **14**, 544–548 (1990)

Qin, Q.H., Mai, Y.W.: Crack growth prediction of an inclined crack in a half-plane thermopiezoelectric solid. Theor. Appl. Fract. Mech. **26**, 185–191 (1997)

Qin, Q.H., Mai, Y.W.: BEM for crack-hole problems in thermopiezoelectric materials. Eng. Fract. Mech. **69**, 577–588 (2002)

Qin, Q.H., Wang, H.: Matlab and C Programming for Trefftz Finite Element Methods. CRC Press, Boca Raton (2008)

Qin, Q.H., Ye, J.Q.: Thermoelectroelastic solutions for internal bone remodeling under axial and transverse loads. Int. J. Solids Struct. **41**, 2447–2460 (2004)

Rashed, Y.F.: BEM for dynamic analysis using compact supported radial basis functions. Comput. Struct. **80**, 1351–1367 (2002a)

Rashed, Y.F.: Dual reciprocity formulation for elasticity problems using compact supported radial basis functions. In: Breebia C.A., Tadeu A., Popov V. (eds.) Boundary Elements XXIV: Incorporating Meshless Solutions, pp. 381–393. WIT Press, Southampton (2002b)

Sadd, M.H.: Elasticity: Theory, Applications, and Numerics. Academic Press, Oxford (2014)

Tsai, C.C.: Meshless BEM for three-dimensional stokes flows. Comput. Model. Eng. Sci. **3**, 117–128 (2001)

Wang, H., Qin, Q.H.: A meshless method for generalized linear or nonlinear Poisson-type problems. Eng. Anal. Bound. Elem. **30**, 515–521 (2006)

Wang, H., Qin, Q.H.: Some problems with the method of fundamental solution using radial basis functions. Acta Mech. Solida Sin. **20**, 21–29 (2007)

Wang, H., Qin, Q.H.: Meshless approach for thermo-mechanical analysis of functionally graded materials. Eng. Anal. Bound. Elem. **32**, 704–712 (2008)

Wang, Z.K., Zheng, B.L.: The general solution of three-dimensional problems in piezoelectric media. Int. J. Solids Struct. **32**, 105–115 (1995)

Wendland, H.: Piecewise polynomial, positive definite and compactly supported radial functions of minimal degree. Adv. Comput. Math. **4**, 389–396 (1995)

Wendland, H.: Error estimates for interpolation by compactly supported radial basis functions of minimal degree. J. Approx. Theory **93**, 258–272 (1998)

Wendland, H.: Scattered Data Approximation. Cambridge University Press, Cambridge (2005)